Experimental Limits on the Dark Matter Halo of the Galaxy from Gravitational Microlensing

C. Alcock,[1,2] R. A. Allsman,[3] T. S. Axelrod,[1,4] D. P. Bennett,[1,2] K. H. Cook,[1,2] K. C. Freeman,[4] K. Griest,[2,5] J. A. Guern,[2,5] M. J. Lehner,[2,5] S. L. Marshall,[2,6] H.-S. Park,[1] S. Perlmutter,[2] B. A. Peterson,[4] M. R. Pratt,[2,6] P. J. Quinn,[4] A. W. Rodgers,[4] C. W. Stubbs,[2,6,7] and W. Sutherland[2,8]

(MACHO Collaboration)

[1]*Lawrence Livermore National Laboratory, Livermore, California 94550*
[2]*Center for Particle Astrophysics, University of California, Berkeley, California 94720*
[3]*Supercomputing Facility, Australian National University, Canberra, A.C.T. 0200, Australia*
[4]*Mount Stromlo and Siding Spring Observatories, Australian National University, Weston, A.C.T. 2611, Australia*
[5]*Department of Physics, University of California, San Diego, California 92093*
[6]*Department of Physics, University of California, Santa Barbara, California 93106*
[7]*Departments of Astronomy and Physics, University of Washington, Seattle, Washington 98195*
[8]*Department of Physics, University of Oxford, Oxford OX1 3RH, United Kingdom*

(Received 23 January 1995; revised manuscript received 13 March 1995)

We monitored 8.6×10^6 stars in the Large Magellanic Cloud for 1.1 years and have found three events consistent with gravitational microlensing. We place strong constraints on Galactic halo lensing objects in the mass range $10^{-4}M_\odot$ to $10^{-1}M_\odot$. Three events are fewer than expected for a standard spherical halo of objects in this mass range, but appear to exceed the number expected from known Galactic populations. Fitting a naive spherical halo model to our data yields a MACHO fraction f of massive compact halo objects (MACHOs), $f = 0.19^{+0.16}_{-0.10}$, a total MACHO mass (inside 50 kpc) of $7.6^{+6}_{-4} \times 10^{10}M_\odot$, and a microlensing optical depth $8.8^{+7}_{-5} \times 10^{-8}$ (68% C.L.).

PACS numbers: 95.35.+d, 97.20.Vs, 98.35.Gi, 98.56.Si

There is strong evidence from the observed flat rotation curves of spiral galaxies that such galaxies (including our own) have extensive halos of dark matter [1]. We have undertaken an experiment that uses gravitational lensing to search for the dark matter in our own Galactic halo [2,3]. The experiment is sensitive to lensing by compact objects over a broad range in mass, spanning from $\sim 10^{-7}M_\odot$ to $\sim 10M_\odot$. This mass regime contains a number of plausible dark matter candidates, including brown dwarfs, black holes, and other stellar remnants. Astrophysical objects of primordial elemental abundances are thought to require a minimum mass of $0.08M_\odot$ to ignite hydrogen fusion, so this experiment is sensitive to nonluminous objects that would have escaped detection in existing sky surveys. Furthermore, we note that a Galactic halo composed entirely of baryonic objects is consistent with the nucleosynthesis bounds on cosmic baryon density [4].

As suggested by Paczyński [5], a population of massive compact halo objects (MACHOs) would be detectable by their gravitational "microlensing" influence on background stars. Microlensing refers to the special case of gravitational lensing in which the splitting of the source star into multiple images is too small to be resolved, but the lensing phenomenon causes a change in the apparent brightness of the source which is time dependent due to the relative motion of the Earth, lens, and source. The apparent amplification $A(t)$ of a background star, in the point-source point-lens approximation, is given by [6]

$$A(t) = A[u(t)] = \frac{u^2 + 2}{u\sqrt{u^2 + 4}},$$
$$u(t) = \left[u_{\min}^2 + \left(\frac{2(t - t_{\max})}{\hat{t}}\right)^2\right]^{1/2}, \quad (1)$$

where $\hat{t} = 2r_E/v$ is the time for the lens to move through two Einstein radii (r_E) relative to the undeflected line of sight, $r_E = \sqrt{4GmD/c^2}$, m is the lens mass, $D = D_{\rm lens}(D_{\rm source} - D_{\rm lens})/D_{\rm source}$, and $u(t)$ is the distance between the lens and the line of sight in units of r_E.

Three teams have reported the detection of gravitational microlensing events, and the world total now exceeds fifty events. The observed spectral invariance of events [7] that were detected before peak amplification [8] lends strong support to the microlensing interpretation.

Most of the events have been seen in the direction of the Galactic center [9–11], but the most suitable target for detecting microlensing by Galactic halo objects is the Large Magellanic Cloud (LMC) [12,13], located at galactic longitude and latitude $(280°, -33°)$ at a distance $D_{\rm source} \approx 50$ kpc. For source stars in the LMC the characteristic time scale $\hat{t}$ for microlensing events from a lens of mass m is approximately $130\sqrt{m/M_\odot}$ days. The fraction of stars being lensed at any given time with $A \geq 1.34$ is defined as the optical depth τ, which would be $\sim 5 \times 10^{-7}$ towards stars in the LMC if the halo is entirely composed of MACHOs [5,14].

Since July 1992, we have carried out photometric monitoring of about 8.6×10^6 stars in the LMC using

the 1.27-m telescope at Mount Stromlo Observatory, Australia. The data used here consist of our Year 1 data, namely, 5169 images of the LMC taken between 21 July 1992 and 3 September 1993, each with an exposure time of 300 s. The images are distributed between 22 fields near the center of the LMC [15]. The number of images per field ranges from 140 to 350.

Measurements of the relative brightness of the stars are automatically performed on each frame. A good-quality image of each field is first chosen as a "template," and a list of star positions and magnitudes is generated. All other images are aligned with the template both in position and flux normalization using a set of bright fiducial stars, and a fit is made to the flux of each star, using a point spread function (PSF) determined from the fiducial stars. Each photometric measurement is output with an error estimate and six quality parameters describing the goodness of the PSF fit, the flux contamination from nearby stars, and the fractions of flux masked by defective pixels and cosmic-ray events in the CCD (charge-coupled device) array.

The dual passband time series for each star is then searched for events consistent with gravitational microlensing. We use empirically determined cuts on the photometry quality flags, along with the associated data such as seeing and sky brightness for each image, to exclude questionable data points, and we also exclude very red stars which are often irregular variables. The remaining light curves are then convolved with a set of filters, and any light curve showing a peak at a modest significance level is defined as a "trigger." For these triggers, a five-parameter least-squares fit to microlensing is made, defined by $\mathcal{F}_B(t) = A(t)\mathcal{F}_{0B}$ and $\mathcal{F}_R(t) = A(t)\mathcal{F}_{0R}$, where $A(t)$ is given in Eq. (1). The fit parameters are the time of peak amplification $t_{\max}$, the characteristic time scale $\hat{t}$, the peak amplification $A_{\max} = A(u_{\min})$, and the base line flux of the star in red and blue passbands $\mathcal{F}_{0R}$ and $\mathcal{F}_{0B}$.

The events passing the trigger are subject to a variety of cuts. We discarded stars whose central pixel typically gets more flux from neighboring stars than from itself. This removes stars with suspect photometry. We also remove stars with $V < 17.5$ as these stars will contribute less than 1% of our detected microlensing events, and they contain a class of variable stars that bear some resemblance to microlensing events. One of our most important cuts is on the improvement in χ^2 of the microlensing fit over a constant flux fit:

$$\Delta\chi^2 \equiv (\chi^2_{\rm ml} - \chi^2_{\rm const})/(\chi^2_{\rm ml}/N_{\rm DF}) > 200,$$

where $N_{\rm DF}$ denotes the number of degrees of freedom. We also demand that the fit $A_{\max}$ exceed both 1.5 and (1+ twice the average estimated error). We further require $\chi^2_{\rm ml}/N_{\rm DF} < 3$, $\chi^2_{\rm ml}/N_{\rm DF} < 4$ in the region of the peak, $\hat{t} < 250$ days, the light curve FWHM < 100 days, and that there be at least three measurements on each of the rising and falling portions of the light curve. Further details and justification for these cuts are presented in [16].

There are four light curves from our Year 1 data that pass the above cuts. Two of these represent the same star detected independently in a field overlap; thus we have three events consistent with microlensing, shown in Fig. 1. The fit parameters are listed in Table I.

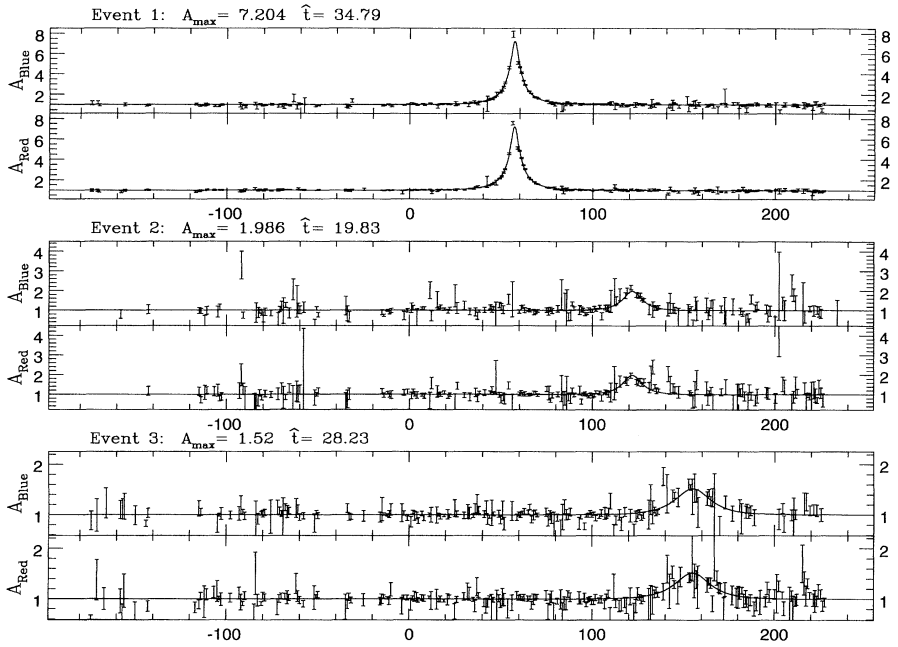

FIG. 1. The three observed stellar light curves that we interpret as gravitational microlensing events are each shown in relative flux units (red and blue) vs time in days. The solid lines are fits to the theoretical microlensing shape using the parameters given in Table I.

TABLE I. Parameters of the events. Columns 4 and 5 show approximate magnitude and color of the lensed stars. Typical uncertainties are ~0.1 mag. Columns 6–8 show the parameters of the best-fit microlensing models: time of peak amplification (Julian days − 2 449 000), the event duration $\hat{t}$, and the peak amplification factor, with the *formal* one sigma errors (derived from the covariance matrix of the fit). Column 9 is the χ^2 per degree of freedom for the microlensing fit.

Event	Right ascension (2000)	Declination (2000)	V	$V - R$	t_{max} (days)	$\hat{t}$ (days)	A_{max}	χ^2
1	05 14 44.5	−68 48 00	19.6	0.6	57.16 ± 0.02	34.8 ± 0.2	7.20 ± 0.09	1.34
2	05 22 57.0	−70 33 14	20.7	0.4	121.62 ± 0.3	19.8 ± 1.3	1.99 ± 0.06	1.41
3	05 29 37.4	−70 06 01	19.4	0.3	154.8 ± 0.9	28.2 ± 1.7	1.52 ± 0.03	1.01

Quantitative interpretation of our results depends upon the event detection efficiency of the experiment. Inefficiencies arise because of (1) the incomplete sampling of the light curves (primarily due to weather interruptions) and (2) the unresolved blending of two or more stars in an image, only one of which will be lensed. In the case of blending, the efficiency per target is reduced because of distortion of the light curve and dilution of the amplification; at the same time, the number of real target objects is increased, which increases the effective efficiency. These two effects partially offset each other.

We calculate the blending efficiency by adding artificial stars into real images and measuring the photometric response to stellar brightenings. Artificial events are then constructed using this detailed knowledge to introduce appropriately degraded microlensing signals into real photometry. These events are then subjected to the same analysis cuts as the real data, yielding our efficiency to detect microlensing on individual stars. We use estimates of the stellar luminosity function (LF) to determine the photometric efficiencies shown in Fig. 2. The two lower curves incorporate the blend efficiencies but use two different LFs. The lowest curve uses the measured LF of "stars" seen in an uncrowded field. The middle curve is based upon a plausible extrapolation of this LF to fainter stars than we can routinely detect, and is the "best estimate" used in this Letter. The upper curve shows only sampling efficiency, and is an upper bound. A more detailed description of this analysis as well as the LFs mentioned above can be found in [16].

In order to illustrate the implications of this result we have compared the number and time scales of the observed events with predictions of the commonly used spherical model [1] of the density of dark matter in the Galaxy's halo,

$$\rho_H(r) = \rho_0 \frac{r_0^2 + a^2}{r^2 + a^2}, \qquad (2)$$

where r is the galactocentric radius, $r_0 = 8.5$ kpc is the galactocentric radius of the Sun, $a = 5$ kpc is the halo core radius, and $\rho_0 = 0.0079 M_\odot\ \mathrm{pc}^{-3} = 0.30\ \mathrm{GeV\,cm}^{-3}$ is the local dark matter density. This model gives a Galactic halo mass of $4.1 \times 10^{11} M_\odot$ within 50 kpc of the Galactic center, and predicts a microlensing rate of $\Gamma = 1.6 \times 10^{-6}(m/M_\odot)^{-0.5}$ (events/star)/yr [14]. After incorporating the detection efficiency, the predicted number of detected events $N_{exp}(m)$ for a dark halo entirely composed of compact objects with a unique mass m is shown in Fig. 3. There are two ways to interpret our results. First, we can conservatively interpret all three events as background and use Poisson statistics to rule out at 95% C.L. all halo models which predict in excess of 7.7 events. Defining $\psi(m)dm$ as the mass fraction of halo Machos with masses between m and $m + dm$, Fig. 3 shows that models with $\psi(m)$ equal to a delta function are ruled out for masses between $m_{low} = 8 \times 10^{-5} M_\odot$ and $m_{high} = 0.3 M_\odot$. In fact, a model with *any* mass distribution restricted to this excluded mass range is also ruled out, since $N_{exp}(m) > 7.7$ implies $N_{exp} = \int_{m_{low}}^{m_{high}} \psi(m) N_{exp}(m) dm > [7.7 \int_{m_{low}}^{m_{high}} \psi(m) dm = 7.7]$. So lens objects in the above mass range cannot contribute 100% of the model halo at 95% C.L. Taking our result in conjunction with the null results from the EROS Collaborations's CCD experiment [17], these two microlensing experiments have placed strong constraints on a dark halo of lensing objects of the form given by Eq. (2) for masses between $5 \times 10^{-8} M_\odot$ and $0.3 M_\odot$.

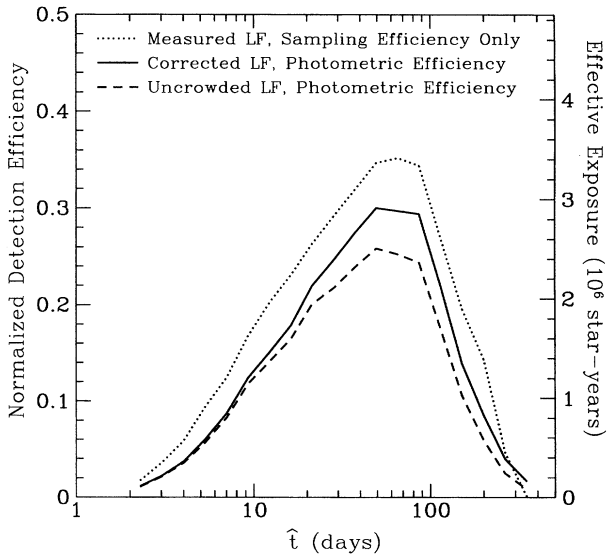

FIG. 2. MACHO Year 1 microlensing event detection efficiency. Here $\mathcal{E}$, normalized to $u_{min} < 1$, is shown as a function of $\hat{t}$, the event duration. The left axis is labeled with event detection efficiency per monitored object, and the right axis gives the efficiency-corrected exposure. The upper curve takes into account only the temporal sampling effects while the lower two correct for event degradation from blending by using two different stellar LFs to estimate the increased number of targets. The best estimate is the middle curve.

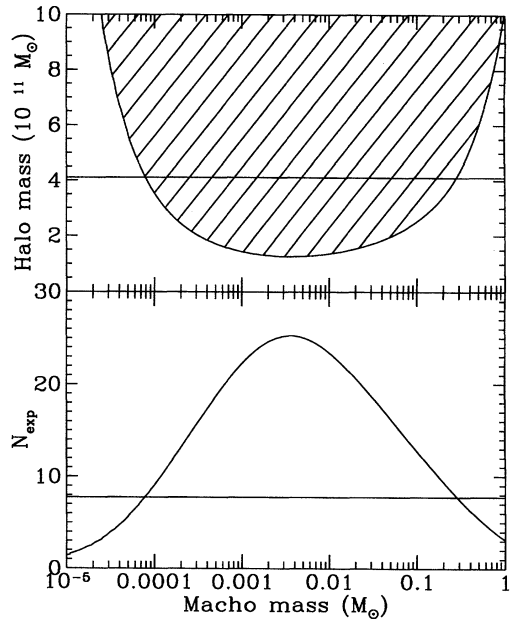

FIG. 3. The lower panel shows the number of expected events predicted from the standard model halo with a delta function mass distribution. Given three observed events, points above the line drawn at $N_{\rm exp}(m) = 7.7$ are excluded at the 95% C.L. The upper panel shows the 95% C.L. limit on the halo mass in MACHOs within 50 kpc of the Galactic center for the model. Points above the curve are excluded at 95% C.L. while the line at $4.1 \times 10^{11} M_\odot$ shows the total mass in this model within 50 kpc.

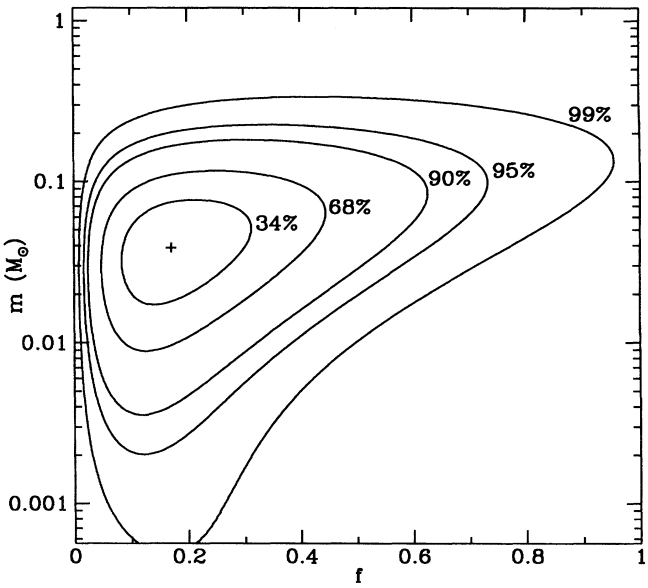

FIG. 4. Likelihood contours for the model halo with a delta function mass distribution. The numbers labeling the contour levels indicate the total probability of the enclosed parameter region according to a Bayesian analysis assuming logarithmic and linear prior distributions in m and f, respectively. The position of the most likely MACHO mass m_{2D} and MACHO halo fraction f_{2D} is marked with a +.

Current estimates [18] of the total Galactic mass within 50 kpc range from 3 to $6 \times 10^{11} M_\odot$, while the model halo of Eq. (2) contains $4.1 \times 10^{11} M_\odot$. Using the 95% C.L. limits on $N_{\rm exp}(m)$ we can set a 95% C.L. upper limit on the mass in this model halo of $M_{\rm lim}(m) = 4.1 \times 10^{11}[7.7/N_{\rm exp}(m)] M_\odot$. As shown in Fig. 3, objects in the mass range $3 \times 10^{-4} M_\odot < m < 0.06 M_\odot$ contribute no more than 50% of the model halo's mass within 50 kpc.

We have explored a range of different halo density profiles [16], and we find that while the constraint on the halo mass *fraction* in MACHOs is quite model dependent our constraints on the *total* mass of MACHOs interior to 50 kpc are relatively independent of the assumed model of the Galactic halo.

In setting the limits above we need not assume that our three events are due to microlensing by halo objects; however, if we add this assumption we can use the observed durations of the events in a maximum likelihood analysis to find the most likely MACHO fraction f and mass m (again with a delta function mass distribution). In this model the rest of the halo is presumed to consist of objects with masses outside our range of sensitivity. Figure 4 shows the likelihood contours with most likely values of $f_{2D} = 0.17$ and $m_{2D} = 0.04 M_\odot$. To find a one-dimensional confidence interval for f we integrate the likelihood function over m and find $f_{\rm ML} = 0.19^{+0.16}_{-0.10}$, where the errors are 68% C.L.

The model of Eq. (2) predicts an optical depth of $\tau_{\rm model} = 4.7 \times 10^{-7}$. Using $f_{\rm ML}$ we can now state the model best fit optical depth of $8.8^{+7}_{-5} \times 10^{-8}$ and observed MACHO mass within 50 kpc of $7.6^{+6}_{-4} \times 10^{10} M_\odot$. We can also estimate the optical depth directly using our observed time scales, our exposure $E = 9.72 \times 10^6$ star years, and efficiencies by computing $\tau_{\rm est} = (\pi/4E) \sum[\hat{t}_i / \mathcal{E}(\hat{t}_i)] = 8.0 \times 10^{-8}$, in good agreement with the maximum likelihood estimate.

It is possible that the observed events, if microlensing, might be due to objects in the LMC [19] or nonhalo Galactic population [20]. We have estimated [16] the event rates due to known stars in the Galactic disk, the spheroid, and the LMC disk and find that they should contribute on average $\sim \frac{1}{2}$ an event to our sample of 3. For three detected events, the 90% C.L. lower bound on the underlying rate is 1.1 events. Note that recent microlensing results toward the Galactic bulge suggest that the standard Galactic models used to predict microlensing may be incorrect [9–11]. Our ongoing observations should help clarify the significance of this difference.

We are grateful for the support given our project by the technical staff at the Mt. Stromlo Observatory. Work performed at LLNL is supported by the DOE under Contract No. W-7405-ENG. Work performed by the

Center for Particle Astrophysics personnel is supported by the NSF through Grant No. AST 9120005. The work at MSSSO is supported by the Australian Department of Industry, Science and Technology. K. G. acknowledges a DOE OJI grant. C. W. S. acknowledges the generous support of the Packard Foundation, and both K. G. and C. W. S. are grateful to the Sloan Foundation for their support.

[1] K. Ashman, Pub. Astron. Soc. Pacific **104**, 1109 (1992); J. Primack, D. Seckel, and B. Sadoulet, Annu. Rev. Nucl. Part. Sci. **B38**, 751 (1988).
[2] C. Stubbs *et al.,* Proc. SPIE Int. Soc. Opt. Eng. **1900**, 192 (1993).
[3] C. Alcock *et al.,* in *Robotic Telescopes in the 1990's,* edited by A. Filippenko (Astronomical Society of the Pacific, San Francisco, 1992).
[4] M. S. Smith, H. K. Lawrence, and R. A. Malaney, Astrophys. J. Suppl. **85**, 219 (1993); C. Copi, D. Schramm, and M. Turner, Science **267**, 192 (1995).
[5] B. Paczyński, Astrophys. J. **304**, 1 (1986).
[6] S. Refsdal, Mon. Not. R. Astron. Soc. **128**, 295 (1964).
[7] S. Benetti, L. Pasquini, and R. M. West, ESO Report No. 1059, 1994.
[8] C. Alcock *et al.,* IAU Telegram 6068 (1994); C. Alcock *et al.,* IAU Telegram 6095 (1994).
[9] A. Udalski *et al.,* Acta Astronomica **44**, 165 (1994).
[10] C. Alcock *et al.,* Astrophys. J. (to be published).
[11] D. Bennett *et al.,* in Proceedings of the 5th Annual Maryland Conference, edited by S. Holt (to be published).
[12] C. Alcock *et al.,* Nature (London) **365**, 621 (1993).
[13] E. Aubourg *et al.,* Nature (London) **365**, 623 (1993).
[14] K. Griest, Astrophys. J. **366**, 412 (1991).
[15] See World Wide Web page http://meteor.anu.edu.au/ ~pjq/macho.html for information of field centers and events in progress.
[16] C. Alcock *et al.* (to be published).
[17] E. Aubourg *et al.,* Astron. Astrophys. (to be published).
[18] K. C. Freeman, in *Unsolved Problems of the Milky Way,* edited by L. Blitz (Kluwer Academic, Dordrecht, 1995), IAU Symp. 169.
[19] X. Wu, Astrophys. J. **435**, 66 (1994); K. C. Sahu, Nature (London) **370**, 275 (1994).
[20] A. Gould, J. Miralda-Escude, and J. Bahcall, Astrophys. J. Lett. **423**, L105 (1994).